Applied Catalysis B: Environmental 241 (2019) 461–470

Contents lists available at ScienceDirect

Applied Catalysis B: Environmental

journal homepage: www.elsevier.com/locate/apcatb

Novel conjugated organic polymers as candidates for visible-light-driven photocatalytic hydrogen production

Jian Chen[a,b,1], Xiaoping Tao[a,c,1], Lin Tao[a,b], He Li[a], Chunzhi Li[a,b], Xiuli Wang[a], Can Li[a], Rengui Li[a,*], Qihua Yang[a,*]

[a] State Key Laboratory of Catalysis, iChEM, Dalian Institute of Chemical Physics, Chinese Academy of Sciences, 457 Zhongshan Road, Dalian, 116023, China
[b] University of Chinese Academy of Sciences, Beijing, 100049, China
[c] School of Chemistry and Materials Science, University of Science and Technology of China, Hefei 230026, China

ARTICLE INFO

Keywords:
Photocatalysis
Conjugated organic polymer
Visible light
Hydrogen production

ABSTRACT

Artificial photosynthesis aiming to capture and convert renewable solar energy into solar fuels (e.g., hydrogen, chemicals) provides a blueprint for sustainable and carbon-neutral world. In artificial photosynthesis, developing novel semiconductors for visible-light-driven photocatalytic water splitting is one of the most demanding challenges. Herein, we designed and explored two kinds of novel bipyridine-based covalent organic polymers, Bp-COP (2,2′-bipyridine-5,5′-diamine: Bp-NH_2) and BpZn-COP (2,2′-bipyridine-5,5′-diamine Zn complex: Bp-Zn), both of which exhibit excellent light-harvesting properties with absorption edges expanding to larger than 600 nm and have appropriate band structures for water splitting. Polymers Bp-COP and BpZn-COP are found to enable efficient photocatalytic hydrogen production under visible light irradiation with Pt as the proton reduction cocatalyst. Further assembling conjugated organic polymers with TiO_2 as charge transferring mediate can remarkably boost their photocatalytic activities to more than 8 times (1333 vs. 162 μmol g^{-1} h^{-1}), giving an apparent quantum efficiency (AQE) of over 2.5% at the input wavelength of 420 nm. This work not only presents a methodology for designing and synthesizing novel organic-based polymers, but also provides promising candidates for potential applications in solar energy conversion.

1. Introduction

Artificial photosynthesis aiming to capture and convert renewable solar energy into solar fuels (e.g., hydrogen, chemicals) provides a blueprint for sustainable and carbon-neutral world [1–6]. The development of semiconductors that possess visible-light responsive absorptions and suitable band structures for photocatalytic water splitting is among the most demanding and long-standing challenges in artificial photosynthesis [7–12]. Compared with numerous inorganic semiconductor photocatalysts reported in the last few decades, organic semiconductor photocatalysts with appropriate energy levels that enable photocatalytic water splitting are much less explored [13–18]. “Graphitic carbon nitride” (g-C_3N_4) is the most famous organic semiconductor photocatalyst and attracts significant attention in photocatalysis [19–28]. However, g-C_3N_4 and its derivatives are invariably composed of heptazine or triazine units, thus offering only limited chemical varieties, which restricts the fine-tuning of their structures and properties [29,30]. Additionally, the utilization of solar photons in visible light region is also largely limited by their relatively wide band gaps.

Conjugated organic polymers (COPs), e.g. covalent organic frameworks (COFs), have been emerging as an intriguing class of photocatalysts, owing to their tailorable electronic and optical properties due to the diverse synthetic modularity [29,31–35]. Indeed, COPs have received more and more attentions in the field of photocatalysis and optoelectronics [36–40]. Recently, several COFs have been employed for visible-light-driven photocatalytic hydrogen evolution. Vyas et al. reported that azine-linked COFs with an absorption edge at ~470 nm could enable photocatalytic hydrogen evolution, however, only ultraviolet light and blue parts of the visible light region could be used due to its relatively wide band gap [41]. Pachfule et al. successfully synthesized chemically stable diacetylene functionalized β-ketoenamine COFs as photocatalyst for photocatalytic hydrogen generation, but the photocatalytic activity is still not high [42]. Cooper and his co-workers reported a series of tunable COPs as photocatalysts for visible-light-driven hydrogen evolution [30–43]. Yu et al. also synthesized COPs

* Corresponding authors.
E-mail addresses: rgli@dicp.ac.cn (R. Li), yangqh@dicp.ac.cn (Q. Yang).
[1] These authors contributed equally to this work.

https://doi.org/10.1016/j.apcatb.2018.09.011
Received 12 June 2018; Received in revised form 21 July 2018; Accepted 4 September 2018
Available online 05 September 2018
0926-3373/

incorporated with light harvesting chromophores, which are capable for photocatalytic H_2 production [44]. Though some progresses have been made using COPs or COFs as organic semiconductors for photocatalytic water splitting, it still desiderates for exploring COPs possessing wide range visible-light absorptions and suitable band structures for efficient solar hydrogen production. However, the developing of novel organic semiconductor with apposite visible light absorption properties and band structures of COPs for solar energy utilization still remains a challenge, and factors affecting their photocatalytic performance have not been investigated in details yet.

Herein, we presented the design and synthesis of semi-crystallized bipyridine-based COPs (Bp-COP), which possess excellent visible-light harvesting capacity and enable efficient photocatalytic H_2 evolution under visible light irradiation. Metallization of Bp-COP with Zn (II) (BpZn-COP) could effectively expand the visible light absorption edge from ~550 nm to more than 600 nm, meanwhile promoting the separation and transportation of photogenerated charges. The photocatalytic activity of BpZn-COP could be further remarkably boosted via assembling them with TiO_2 nanoparticles due to fast transferring of photogenerated electrons from polymers to conduction band of TiO_2, which was verified via in-situ visible light photodeposition probe reactions and time-resolved photoluminescense characterizations. The bipyridine-based conjugated organic polymers are demonstrated to be promising candidates for potential applications in solar energy conversion.

2. Experimental

2.1. Materials and general procedures

1,3,5-tri(3′-tert-butyl-4′-hydroxy-5′-formylphenyl (TTHB) was prepared according to the reference [45]. 2,2′-bipyridine-5,5′-diamine (Bp-NH_2) was purchased from Jilin Province In-depth Research Technology Co., Ltd. (China). Zinc bromide ($ZnBr_2$) were obtained from Aladdin Co. China. Other reagents were of analytical grade and used without further purification.

2.2. Characterizations

Nitrogen sorption isotherms were collected on a Micromeritics ASAP 2020 system volumetric adsorption analyzer at 77 K. Before the sorption measurements, the samples were degassed at 100 °C for 12 h. The BET surface area was calculated from the adsorption data at a relative pressure P/P_0 in the range of 0.04–0.20. Pore size distributions were determined from a nonlocal density functional theory (NLDFT) method. C, H, N elemental analysis was performed with an Oxygen/Nitrogen/Hydrogen Analyzer (EMGA-930, HORIBA, Japan) and a Carbon/Sulfur Analyzer (EMIA-8100, HORIBA, Japan). TGA was performed from 30 to 900 °C with a heating rate of 5 °C min^{-1}, using a NETZSCH STA 449F3 analyzer under air atmosphere. FT-IR spectra in the range of 400–4000 cm^{-1} were collected with a Nicolet Nexus 470 IR spectrometer using KBr pellets. High resolution transmission electron microscopy (HRTEM) images were recorded on a FEI Tecnai F30 microscope with a point resolution of 0.20 nm operated at 300 kV. Scanning electron microscopy (SEM) was undertaken using a FEI Quanta 200 F scanning electro-microscope, operating at an acceleration voltage of 2–30 kV. Transmission electron microscopy (TEM) was performed on a HITACHI 7700, at an acceleration voltage of 100 kV. Solid-state NMR spectra were obtained with a Bruker 500 MHz spectrometer equipped with a magic-angle spin probe using a 4 mm ZrO_2 rotor. ^{13}C signals were referenced to glycine ($C_2H_5NO_2$). The experimental parameters were as follows: 8 kHz spin rate, 5 s pulse delay, and 2500 scans. Photoluminescence spectra were recorded on an FLS920 fluorescence spectrometer (Edinburgh Instruments) in air at room temperature. A Xe lamp and a picosecond pulsed diode laser (406.8 nm) were used as the excitation source. The UV–vis spectra were collected with a ShimadzuUV-Vis 2550 spectrophotometer. Zinc content were determined by PLASAM-SPEC-II inductively coupled plasma atomic emission spectrometry (ICP), by digesting the polymer in HNO_3/H_2SO_4 (1:1, v/v). Cyclic voltammetry (CV) measurement was performed using an CH Instruments Model 760E electrochemical work station (CHI760E). Glassy carbon electrode drop-casted with the polymers as the working electrode, Pt wire as the counter electrode, $Ag/AgNO_3$ (in 0.1 M $AgNO_3$ acetonitrile solution) electrode as the reference electrode, Bu_4NPF_6 (0.1 M in acetonitrile) was used as electrolyte. The reduction potential was recorded with a scan rate of 50 mV/s. For calibration, the redox potential of ferrocene/ferrocenium (Fc/Fc^+) was measured under the same conditions. *LUMO* energies of these conjugated polymers were estimated with the following equations:

$$LUMO = -e[4.8 - E_{ox,onset}^{Fc/Fc^+} + E_{red,onset}^{Sample}]$$

The corresponding *HOMO* levels were calculated by subtracting the *LUMO* level from the optical band gap.

2.3. Synthesis of BpZn-COP and Bp-COP

In a typical experiment for the preparation of Bp-COP-Zn, the synthesis of metal complex (Bp-Zn) by Bp-NH_2 and $ZnBr_2$ was based on previous reference, [46,47].

2 mL THF contained 0.3 mmol (180 mg) TTHB was transferred to 10 mL stainless autoclave with 500 rpm stirring speed. Then 0.5 mL DMF solution contained 0.45 mmol Bp-Zn was added to the stainless autoclave. The stainless autoclave was heated to 100 °C for 3 days in oven. Then the reaction was cooled to room temperature. The golden red color powder Bp-COP-Zn with yield 58% was obtained after filtering and washing with THF and CH_2Cl_2. At last the powder was dried in 60 °C oven for 12 h. Elemental analysis (%): C 51.2, H 5.0, N 8.1. ICP (Zn): 5.6 wt% (Table 1).

As for synthesis of Bp-COP polymer, 2 mL THF contained 0.3 mmol (180 mg) TTHB was transferred to 10 mL stainless autoclave with 500 rpm stirring speed. Then 0.5 mL DMF solution contained 0.45 mmol Bp-NH_2 and 0.6 mL 3 M acetic acid were added to the stainless autoclave at the same time. The stainless autoclave was also kept into 100 °C oven for 3 days. The Bp-COP with yield 68% was obtained after filtering and washing with THF and CH_2Cl_2. Elemental analysis (%): C 61.0, H 5.2, N 8.7 (Table 1).

2.4. Synthesis of BpZn-COP (3 wt.% Pt) and Bp-COP (3 wt.% Pt)

The 50 mg Bp-COP-Zn or Bp-COP solid was dispersed to 10 mL CH_3CH_2OH solution and 2 mL of H_2PtCl_6 aqueous solution (0.8 mg/mL) was added. The mixture solution was stirred with 500 rpm for 1 h and then dried by evaporation under reduced pressure. The collected solid impregnation with H_2PtCl_6 was reduced in a H_2 atmosphere with a flow rate of 30 mL min^{-1} at 200 °C temperature for 2 h with a heating rate of 1 °C min^{-1}. The Bp-COP-Zn with different Pt content (0.5–15 wt.%) was also prepared according to the above method.

2.5. Synthesis of TiO_2@BpZn-COP-x% (x refers to wt.% of BpZn-COP), TiO_2@Bp-COP-2.5%, TiO_2@Bp-COP-2.5% (without Pt) and SiO_2@BpZn-COP-2.5%

Typically, 200 mg of TiO_2 (photo-deposited with 0.5 wt. % Pt) was dispersed in 10 mL of THF in a 25 mL flask. Then the desired amount of

Table 1
Element analysis of Bp-COP and BpZn-COP.

Sample	C (wt%)	H (wt%)	N (wt%)	Zn (wt%)
Bp-COP	61.2	5.2	8.7	–
BpZn-COP	51.2	5.0	8.1	5.6

TTHB and Bp-Zn in stoichiometric ratio was dissolved in mixture solution (1 mL THF/0.5 mL DMF) and added to the flask or tube. The flask was heated to 68 °C with 500 rpm stirring speed for 2 days. Then the solid material was collected by filtering and washing with organic solvent THF and EtOH, the solid material was denoted to TiO_2@Bp-COP-Zn-x% (the x value according to total organic monomers weight percentage to TiO_2). TiO_2@Bp-COP-2.5% was also prepared by the above method.

TiO_2@BpZn-COP-2.5% (without Pt) was also synthesized by pure TiO_2 composition with BpZn-COP according to the same procedure. This material was used for photodeposition metal particles (Au or Pt) on TiO_2@BpZn-COP-2.5% (TiO_2 without Pt) under visible light ($\lambda \geq 420$ nm) in following experiment.

SiO_2@BpZn-COP-2.5% was prepared by using SiO_2 sphere (with 0.5 wt. % Pt) instead of TiO_2.

2.6. General procedure for photocatalytic hydrogen evolution

Hydrogen evolution was studied under standardized conditions and measured in the presence of TEOA as sacrificial electron donor. Photocatalyst (20 mg) was dispered in solution of 85 mL water/15 mL triethanolamine (TEOA). The photocatalytic H_2 evolution reactions were carried out in a closed gas circulation and evacuation system (perfect light) using a 300 W Xe lamp (Ushio-CERMAX LX300) and optical cutoff filter (kenko, L42; $\lambda \geq 420$ nm). The amount of evolved H_2 was determined by an on-line gas chromatograph (Shimadzu GC-8 A, TCD, Ar carrier). The rate of H_2 evolution in the initial 1 h was used for evaluating the photocatalytic activity of the samples. Apparent quantum efficiency (AQE) for photocatalytic H_2 production under the input wavelength of 420 nm was measured with 50 mg TiO_2@BpZn-COP-2.5% in 150 mL TEOA aqueous solution (15 vol%).

2.7. Experiments for photodeposition metal particles (Au or Pt) on TiO_2@BpZn-COP-2.5% (TiO_2 without Pt) under visible light ($\lambda \geq 420$ nm)

20 mg TiO_2@BpZn-COP-2.5% (TiO_2 without Pt) was dispered in solution of 85 mL water/15 mL triethanolamine (TEOA). A solution containing 3 wt. % metal ion ($HAuCl_4$ or H_2PtCl_6) compared with solid material was added into the system. The photodeposition metal particles (Au and Pt) were carried out by using a 300 W Xe lamp (Ushio-CERMAX LX300) and optical cutoff filter (kenko, L42; $\lambda \geq 420$ nm) for 3 h. Then the solid material with photodeposition metal particles was obtained by centrifugation.

3. Results and discussion

As outlined in Scheme 1, Bp-COP and BpZn-COP were synthesized through the Schiff base condensation reaction of 2,2′-bipyridine-5,5′-diamine (Bp-NH_2) or 2,2′-bipyridine-5,5′-diamine Zn complex (Bp-Zn) with 1,3,5-tri (3′-tert-butyl-4′-hydroxy-5′-formylphenyl) benzene (TTHB) in stainless autoclave at of 100 °C for 3 days. TTHB containing −OH groups was introduced as precursor due to the fact that −OH groups could modulate the band gap of polymers [48].

Powder X-ray diffraction (PXRD) patterns of Bp-COP and BpZn-COP gave sets of diffraction peaks with an intense peak in the low-angle region respectively at 5.48° and 4.16°, indicating that the two polymers possess certain crystallinity. However, no obvious lattice stripes could be observed in the high resolution transmission electron microscopy (HRTEM) image of BpZn-COP (Fig. S1). Efforts to determinate the crystal structure using Materials Studio failed. Consequently, Bp-COP and BpZn-COP only had semi-crystallinity. BpZn-COP mainly had microporous structure as evidenced by its type I N_2 sorption isotherm pattern and Bp-COP had hierarchical micro-mesopore due to the co-existence of type I and type IV N_2 sorption isotherm pattern. The obvious H3 hysteresis loop for Bp-COP suggested the existence of the aggregates of platy particles. The pore size of BpZn-COP centered at 1.3–1.6 nm and that for Bp-COP was very broad (1.3 nm to dozens of nanometers) (Fig. S2). Bp-COP and BpZn-COP had comparable BET surface area of 351 and 354 m^2/g, respectively. According to the TEM and SEM characterizations, Bp-COP was composed of aggregated micro-size polymer particles, while BpZn-COP was consist of microsheets (Fig. 2).

In the FT-IR spectra of Bp-COP and BpZn-COP, the vibration peak of C═N could be clearly observed at 1616 cm^{-1}, showing the condensation of aldehyde and amine group for the formation of polymer. The characteristic −OH stretching vibration could be found at around 3440 cm^{-1}, and the band at 1571 cm^{-1} could be assigned to skeleton vibration of aromatic ring and the bands at ca. 2956 cm^{-1} were due to the C−H stretching vibration. The C═O stretching vibration at 1648 cm^{-1} showed the existence of unreacted aldehydes around the periphery of the polymers. These results have been further corroborated by the solid-state ^{13}C CP-MAS NMR spectra of Bp-COP and BpZn-COP, in which the resonance at 160 ppm was originated from the carbon atom of C═N and aromatic carbon adjacent to the oxygen atom in the phenoxy group while the resonances at 135 and 126 ppm were assigned to the aromatic carbons. The representative signals of quaternary carbons in ^{t}Bu appeared at 34 and 29 ppm. On the basis of the above results, we can draw a conclusion that COPs were successfully constructed through the Schiff-base Chemistry reaction.

In order to further investigate the surface compositions of the COPs, X-ray photoelectron spectroscopy (XPS) was conducted (Fig. 3). The binding energy of N1s for Bp-COP was located at 398.8 eV corresponding to the N atoms of both imine bond (−N═C−) and pyridine unit (−N═C−). Notably, BpZn-COP exhibited a new N1s binding peak at 399.4 eV, attributable to N atom of pyridine unit coordination with Zn (II), strongly suggesting the existence of interactions between Zn(II) and bipyridine moieties in BpZn-COP. The binding energies of Zn $2p_{1/2}$ and Zn $2p_{3/2}$ respectively appearing at 1045.4 and 1022.4 eV clearly showed the presence of Zn (II) in BpZn-COP. The weight amount of Zn in BpZn-COP was measured to be 5.6 wt. % via ICP analysis (Table 1).

Both Bp-COP and BpZn-COP had golden red color apparently (Fig. 4A), suggesting excellent absorptions in visible light region. Diffuse reflectance ultraviolet-visible (UV–vis) spectra of Bp-COP and BpZn-COP confirmed their visible light absorption properties (Fig. 4A). Compared with Bp-COP, BpZn-COP displayed an obvious red-shift from ~550 nm to more than 600 nm and the band gaps were estimated to be 2.18 eV and 2.35 eV for BpZn-COP and Bp-COP, respectively (Fig. S3). The red-shift of absorption edge may be attributed to the coordinating metal ion Zn(II) in the conjugated organic polymer framework, which affects the electronic transition property of organic framework. The extending absorption edge is benefit to utilize visible light of solar energy. The energy levels of Bp-COP and BpZn-COP were measured by cyclic voltammetry method, showing that the LUMO levels of Bp-COP and BpZn-COP were respectively located at −0.77 and −0.76 eV vs. NHE (Fig. 4B and C). Considering the obtained band gaps, the corresponding band structures and energy levels of Bp-COP and BpZn-COP are depicted in Fig. 4D, from which we can deduce that both polymers possess appropriate energy levels for potential applications in photocatalytic water splitting, especially for their negative enough LUMO levels for protons reduction for hydrogen evolution.

Phtocatalytic hydrogen production from water splitting was then introduced to evaluate the performances of as-prepared polymers. Fig. 5A depicts the photocatalytic hydrogen evolution over Bp-COP and BpZn-COP under visible light irradiation ($\lambda \geq 420$ nm). Interestingly, both Bp-COP and BpZn-COP are capable for photocatalytic hydrogen production in the presence of Pt as the proton reduction co-catalyst and triethanolamine (TEOA) as sacrificial electron donors. The size of Pt nanoparticles on the surface of COPs was ~3–4 nm based on TEM characterization (Fig. S4). The content of Pt nanoparticles and corresponding photocatalytic activity of BpZn-COP have been investigated. Fig. S5 shows the TEM images of BpZn-COP deposited with different amount of Pt nanoparticles, which clearly displays the increasing

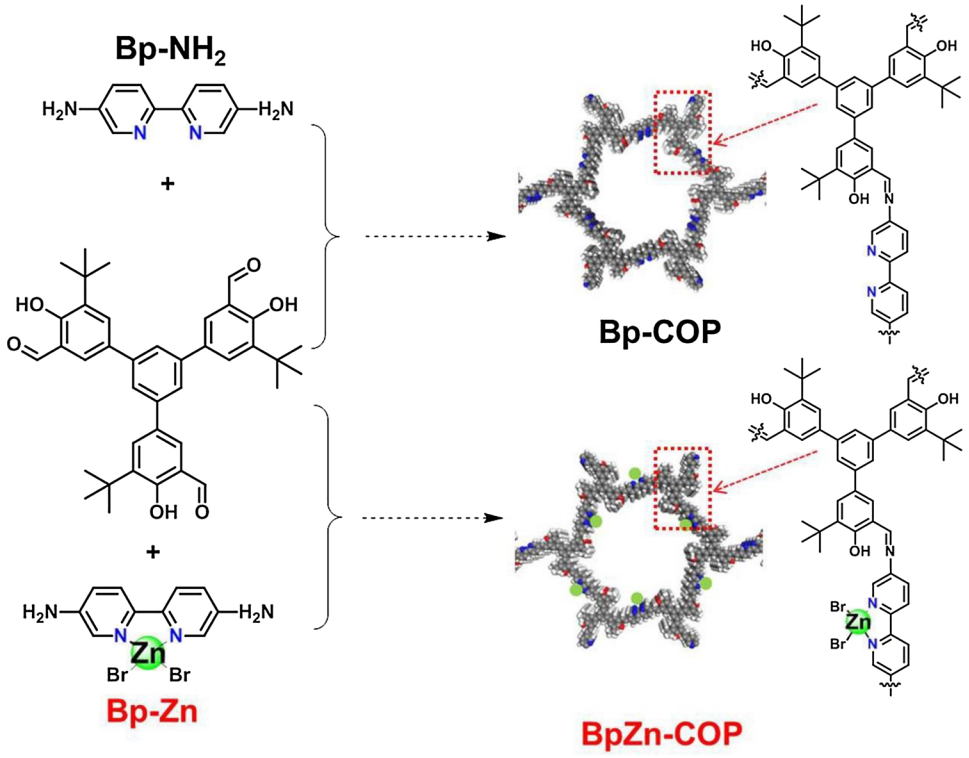

Scheme 1. Schematic illustration for the synthesis of Bp-COP and BpZn-COP.

Table 2
The PL decay lifetimes of BpZn-COP, SiO_2@BpZn-COP and TiO_2@BpZn-COP, fitted from Fig. 7A.

Samples	τ_1 (ns)	A_1(%)	τ_2(ns)	A_2(%)	χ^2	τ_{ave}(ns)
BpZn-COP	0.47	83.27	1.37	16.73	1.35	0.62
SiO_2@BpZn-COP	0.45	77.91	1.35	22.09	1.84	0.65
TiO_2@BpZn-COP	0.20	62.91	0.67	37.09	1.34	0.37

The PL decay time and amplitudes are modeled using a bi-exponential Eq. (1).

number of Pt nanoparticles on BpZn-COP when the content is ranged from 0.5% to 15%. As shown in Fig. S6, the photocatalytic activity is greatly improved as Pt content was increased from 0.5 wt.% to 3.0 wt. %. However, the further increasing the Pt amount on BpZn-COP leads to the decreasing of the photocatalytic activity (Fig. S6), which may be due to the light blocking effect of the exceed amount of Pt nanoparticles on the surface of BpZn-COP. The amount of H_2 production over both polymers increased linearly along with reaction time without any obvious decline in the evaluation period. It is noteworthy that BpZn-COP showed extremely high photocatalytic activity, which was almost one order magnitude than that of Bp-COP, implying that the presence of Zn (II) in the polymer fragment is important for enhancing the photocatalytic activity for hydrogen production. According to the works recently reported (Table S1), both of Bp-COP ($22\,\mu mol\,h^{-1}\ g^{-1}$) and BpZn-COP ($162\,\mu mol\,h^{-1}\ g^{-1}$) give relatively higher photocatalytic activity than pure g-C_3N_4 in hydrogen production under the similar reaction condition, indicating the good property of these two polymers for photocatalytic hydrogen production. We also evaluated the photocatalytic hydrogen production performance of BpZn-COP under different wavelength ranges of incident light, revealing that the trend of photocatalytic activity in different wavelengths is in good consistent with its absorption spectrum (Fig. 5B). The result indicates that all the photoexicted charges in the BpZn-COP possess sufficient energy for photocatalytic hydrogen production and the reaction faithfully proceeded via photoabsorption by the photocatalyst. Fluorescence spectroscopy was then conducted to understand the different photocatalytic behaviors between Bp-COP and BpZn-COP. As shown in Fig. 5C, BpZn-COP revealed an evident decreasing in fluorescence intensity, which was more than 90% decrement than that of Bp-COP. The decreased intensity of fluorescence indicates that bipyridine-Zn(II) complex in the framework of BpZn-COP may render a promoted separation of photoelectrons and holes, which obviously shows the importance of Zn(II) for photogenerated charge separation in the organic polymer [49–52]. To further identify the role of Zn(II) in BpZn-COP in charge separation, Electrochemical Impedance Spectroscopy (EIS) measurements for both Bp-COP and BpZn-COP electrodes were performed (Fig. 5D). R_s is the circuit resistance and R_{ct} represents the charge transfer resistance across the semiconductor-electrolyte interface. The EIS results showed that integrated resistance, including R_s and R_{ct} of BpZn-COP was an order of magnitude lower than that of Bp-COP, implying that the presence of Zn(II) could greatly promote the charge transport inside the bulk as well as the charge transfer across the semiconductor/electrolyte interface. The promoted charge separation and transfer could consequently suppress the electron-hole recombination and improve the utilization efficiency of photogenerated electrons/holes. Based on the above characterizations, the presence of Zn(II) in the framework of polymers is essential for extending absorption edge, ameliorating the separation and transportation of photogenerated charges, resulting in a much higher photocatalytic activity.

A photocatalytic process is generally determined by three main steps: light harvesting, charge separation and surface redox reactions on the photocatalysts. Considering the fact that both Bp-COP and BpZn-COP exhibit excellent light-harvesting properties as described above, their photocatalytic activities may be further improved via manipulating the charge separation and surface reaction processes. Hence, BpZn-COP was assembled with TiO_2, a wide bandgap semiconductor as charge transferring donors by one-pot synthesis method for the preparation of composite photocatalysts, TiO_2@BpZn-COP-x% (x refers to wt. % of BpZn-COP, details see experimental) [53–55]. The presence of characteristic vibration peaks of BpZn-COP in the FT-IR spectrum indicates that the introduction of TiO_2 in TiO_2@BpZn-COP does not obviously affect the composition of BpZn-COP (Fig. S7). The TG analysis

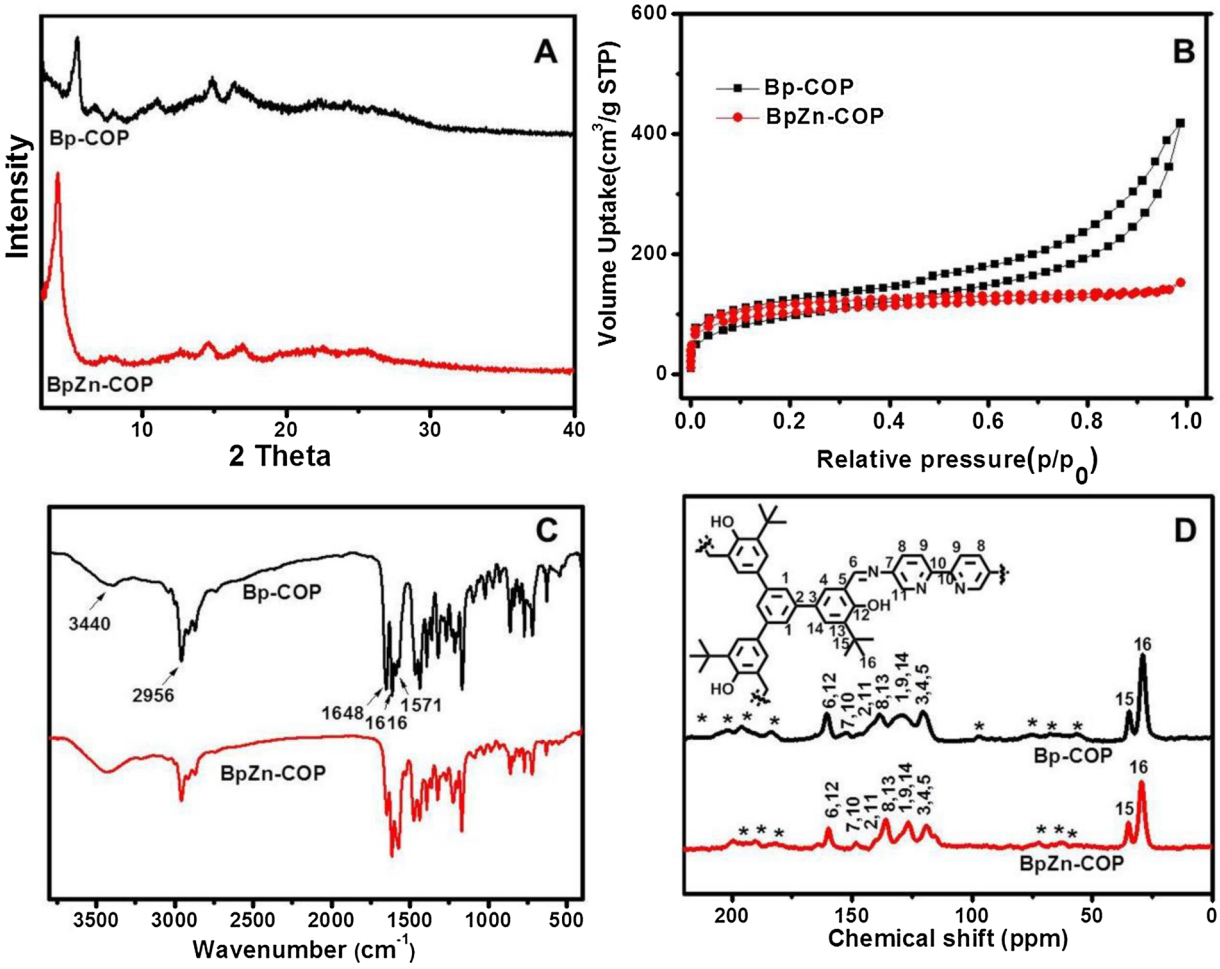

Fig. 1. (A) Powder X-ray diffraction (PXRD), (B) N_2 sorpiton isotherms at 77 K, (C) Fourier transform infrared (FT-IR) spectra and (D) Solid state ^{13}C CP-MAS NMR spectra of Bp-COP and BpZn-COP.

shows that the amount of BpZn-COP in the composites could be facilely varied from 5 wt. % to 70 wt. % (Fig. S7). The TEM images shows that TiO_2 nanoparticles were embedded in the polymer for TiO_2@BpZn-COP-x% with $x \geq 30$, while coated by polymer with $x < 30$ (Figs. 6A and S8). TiO_2@BpZn-COP-x% exhibits an apparent blue shift of light absorption range, which varies by changing the component between the polymer and TiO_2 (Fig. S9). This is possibly due to the low conjugation degree of the polymer in the composites because the visible light absorption properties of BpZn-COP are mainly attributed to the conjugated polymer networks.

The evaluation of photocatalytic performance indicates that all the TiO_2@BpZn-COP-x%composite photocatalysts showed photocatalytic activity for H_2 evolution and the amount of H_2 generated increased linearly along with reaction time (Fig. S10). It was found that the photocatalytic performance of TiO_2@Bp-POF-Zn was prominently improved compared with pure BpZn-COP. The photocatalytic activity of TiO_2@BpZn-COP-x% increased as polymer content decreased and reached the maximum at x of 2.5 (Figs. 6B and S10). TiO_2@BpZn-COP-2.5% with the average thickness of polymer layer around TiO_2 of 3–4 nm afforded the highest photocatalytic activity, which was found to be drastically triggered to be over 8 times than that of BpZn-COP (from 162 to 1333 $\mu mol\, g^{-1}\, h^{-1}$). Further increasing the content of polymer yet led to a decrement in activity, which is possibly due to the fact that too thick polymer layers elongate the distance for photogenerated charges transferring from the polymer to TiO_2. The above results evidently manifest the significant role of TiO_2 in promoting the photocatalytic activity in the composite. Apparent quantum efficiency (AQE) for photocatalytic H_2 production under the input wavelength of 420 nm was then measured, affording out an AQE exceeding 2.5% for TiO_2@BpZn-COP-2.5%. Compared with reported porous organic polymers so far, BpZn-COP should be a potential material for efficient utilization of solar energy. Additionally, photocatalytic activities under different irradiation wavelength regions was evaluated over TiO_2@BpZn-COP-2.5% and the trend of photocatalytic activity in different regions also tracked well with the absorption spectrum (Fig. S11). The promoted photocatalytic performance was also confirmed via assembling TiO_2 with Bp-COP polymer, which showed over 19 times enhancement in photocatalytic activity compared with Bp-COP (22–420 $\mu mol\, g^{-1}\, h^{-1}$) (Fig. 6C). The composite TiO_2@BpZn-COP gives the much higher photocatalytic activity than most of g-C_3N_4 composites recent reported (Table S2), which strongly confirms that the Bp-COP and BpZn-COP exhibit superior performance than g-C_3N_4.

As pristine TiO_2 yielded negligible photocatalytic activity under visible light, the obvious increment in photocatalytic activity of the composite photocatalysts is possibly related with the separation and transfer of photogenerated electrons from polymers to TiO_2. To gain more insight into the roles of TiO_2 in the separating and transferring of photogenerated charges in the composite photocatalyst, time-resolved photoluminescence (TRPL) spectra for BpZn-COP, TiO_2@BpZn-COP-2.5% and SiO_2@BpZn-COP-2.5% (a control sample details see experimental) were performed (Fig.S12, Fig. 7A and Table 2). We found that the PL decay trace of the TiO_2@BpZn-COP exhibited an evident shorter lifetime of the photoluminescence than that of BpZn-COP, implying an the efficient charge transfer from BpZn-COP to the conduction band of

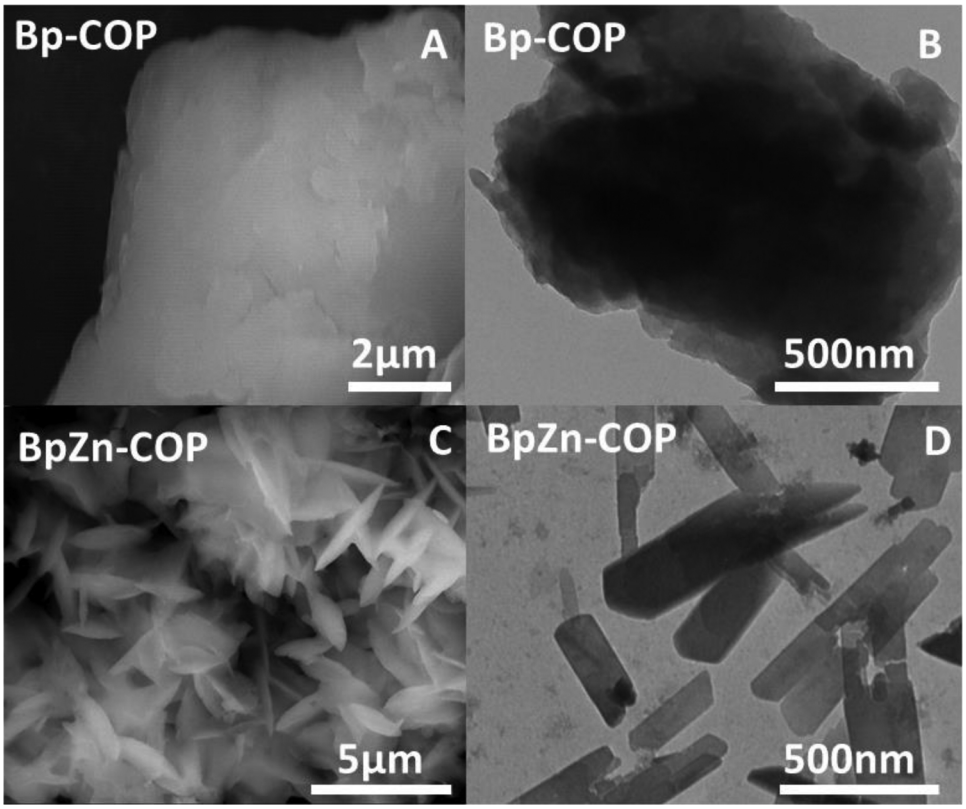

Fig. 2. (A) SEM and (B) TEM images of Bp-COP, (C) SEM and (D) TEM images BpZn-COP.

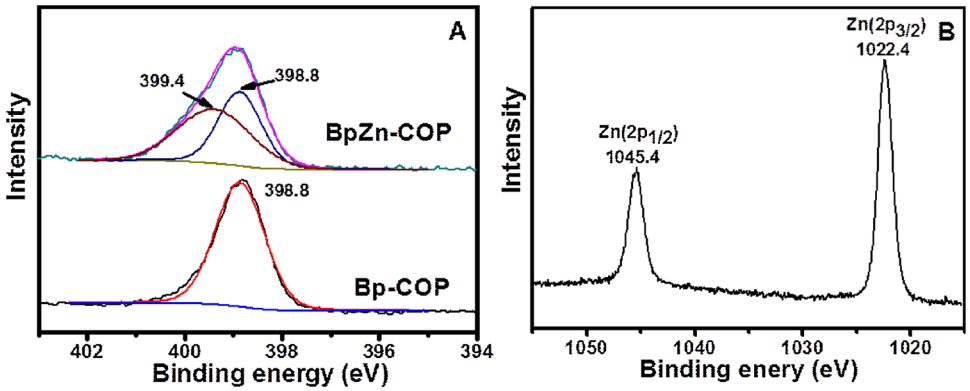

Fig. 3. (A) N1s XPS spectra of BpZn-COP and Bp-COP, (B) Zn2p XPS spectrum of BpZn-COP.

TiO_2 [56–59]. This charge transfering process effectively suppressed the recombination of the photogenerated charges and holes through fluorescence emission. Besides, insulator SiO_2 was also introduced to replace TiO_2 for comparsion. As expected, the SiO_2@BpZn-COP-2.5% gave a nearly same lifetime of photoluminescence to BpZn-COP and no improvement in hydrogen production activity compared with bare polymer. The results indicate the existence of charge transferring from BpZn-COP to TiO_2 and no charge transferring between BpZn-COP and SiO_2. The transferring of photoexicted electrons will increase the probability for more electrons participating in the following surface catalytic reaction and decrease the charge recombination, which contributes to the remarkably enhanced photocatalytic activities.

In order to further confirm the charge separation path between polymer BpZn-COP and TiO_2, in-situ photo-reduction deposition of noble metals (Au, Pt) under visible light ($\lambda \geq 420$ nm) was used as probe reactions to determine the location of photogenerated electrons. As shown in Figs. 7B and S13, Au and Pt nanoparticles were selectively deposited on the interface of BpZn-COP and TiO_2 but not on the outer surface of BpZn-COP, which clearly implies that the photogenerated electrons transferred from BpZn-COP to TiO_2 and accumulated at the polymer/TiO_2 interface. [60] According to N_2 sorption isotherm and pore size distribution data, BpZn-COP material possesses large BET surface (354 m^2/g) and uniform pore size at ~1.3–1.6 nm (Figs. 1 and S2). The high hydrogen evolution activity of TiO_2@BpZn-COP composite confirms that water molecular can indeed smoothly pass through the porous bulk BpZn-COP to the interface of BpZn-COP and TiO_2 then participate the following reaction with photogenerated electrons. Besides, the visible-light-driven Au and Pt nanoparticles deposited on the interface of BpZn-COP and TiO_2 also supports such successful mass transport process. Actually, these experiment results also support the process of photogenerated electrons transferring from bulk BpZn-COP to its surface, which refers to the interface of BpZn-COP and TiO_2 here. Based on the PL and in-situ photodeposition results, we could draw a clear image on the charge separation and transfer from polymers to TiO_2 as illustrated in Fig. 7C. The polymer absorbs visible light and generates photoexcited electrons from HOMO to LUMO which then

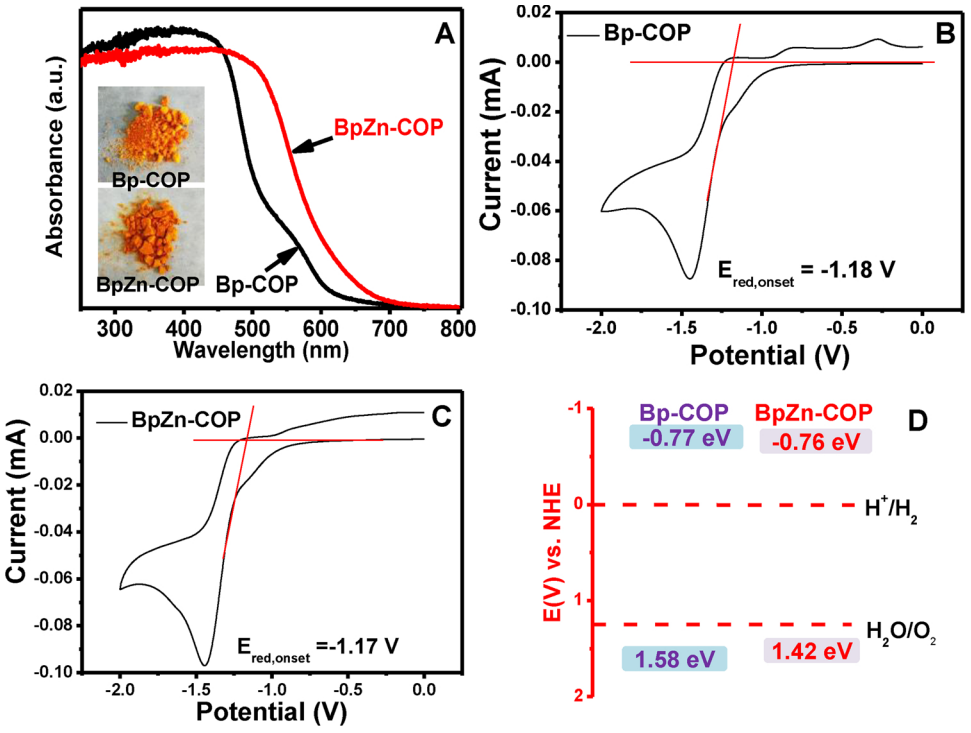

Fig. 4. (A) UV–vis spectra (with sample pictures inset); (C) and (D) Reduction potential of Bp-COP and BpZn-COP measured by cyclic voltammetry. The reduction potential was recorded with a scan rate of 50 mV/s. For calibration, the redox potential of ferrocene/ferrocenium (Fc/Fc^+) was measured under the same conditions. LUMO energies of these conjugated polymers were estimated with the following equations: $LUMO = -e[4.8 - E_{ox,onset}^{Fc/Fc^+} + E_{red,onset}^{Sample}]$; (D) HOMO/LUMO band position measured by cyclic votammetry and optical band gap.

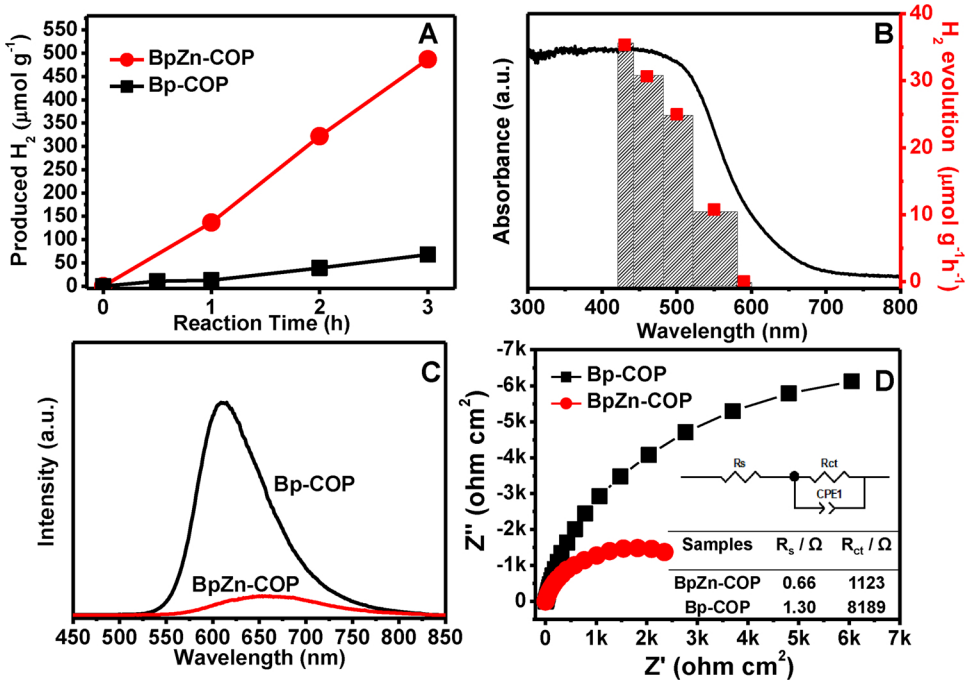

Fig. 5. (A) Visible light ($\lambda \geq 420$ nm) H_2 production with 3 wt. % Pt as co-catalyst and triethanolamine as the sacrificial electron donor, (B) Photocatalytic H_2 evolution under different irradiation wavelength regions over BpZn-COP (3 wt. % Pt), (C) Photoluminescense spectra of Bp-COP and BpZn-COP with excitation wavelength of 350 nm, (D) Electrochemical impedance spectra (EIS) of Bp-COP and BpZn-COP were carried out at the potential of 1.60 V vs. RHE, with an AC potential frequency ranging from 0.1 Hz to 100 kHz on a PARSTAT 2273 workstation (Princeton Applied Research) at room temperature under the irradiation of 365 nm monochromatic LED lamp. In the equivalent circuit (inset), R_s represents the circuit series-resistance, CPE1 is the capacitance phase element of the semiconductor-electrolyte interface, and R_{ct} is the charge transfer resistance across the interface.

transfer to the conduction band of TiO_2 rapidly, leaving the photo-excited holes located at the LUMO levels of the polymers. The spatial separation of photogenerated electrons and holes between polymer and TiO_2 could prolong the lifetime of charge carries and decrease the possibility of charges recombination, thus enhancing the efficiency of solar energy conversion.

$$f(t) = B + \sum_i A_i \exp(-\frac{t}{t_i}) \quad (1)$$

The average PL decay times (τ_{ave}) are estimated using the τ_i and Ai values from the fitted curve data (Table 2) using Eq. (2),

$$\tau_{ave} = \frac{\sum_i A_i \tau_i}{\sum_i A_i} \quad (2)$$

The stability of the polymer BpZn-COP and composite TiO_2@BpZn-COP were also investigated. Fig. S14 shows that the pristine polymer BpZn-COP reveals much stable photocatalytic performance even after 3 cycles. The FT-IR spectrum of the BpZn-COP sample after reaction exhibits the same characteristic vibrations of polymer framework as the fresh sample (Fig. S15), which indicates the stability of polymer framework under the photocatalytic condition. ICP result also shows that the BpZn-COP after 3 cycles still contains 5.27 wt.% Zn, indicating the Zn(II) is quite stable in the organic framework. As shown in Fig. S16,

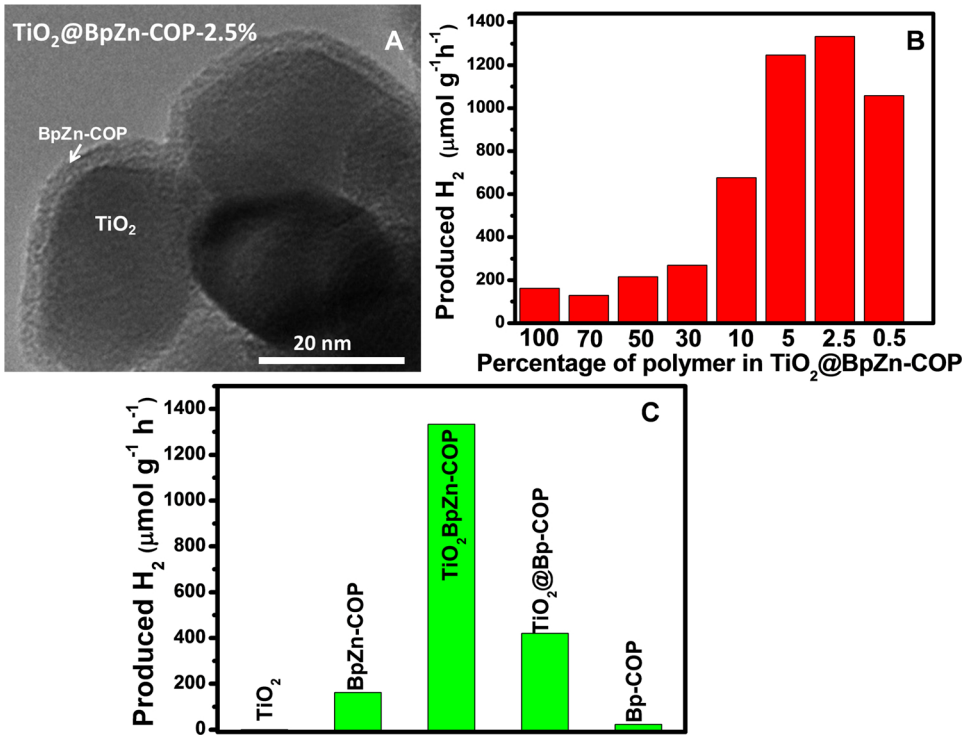

Fig. 6. (A) TEM image of TiO_2@BpZn-COP-2.5%, (B) The photocatalytic H_2 evolution activity of TiO_2@BpZn-COP-x% with triethanolamine as sacrificial electron donor, (C) Photocatalytic H_2 evolution of different samples.

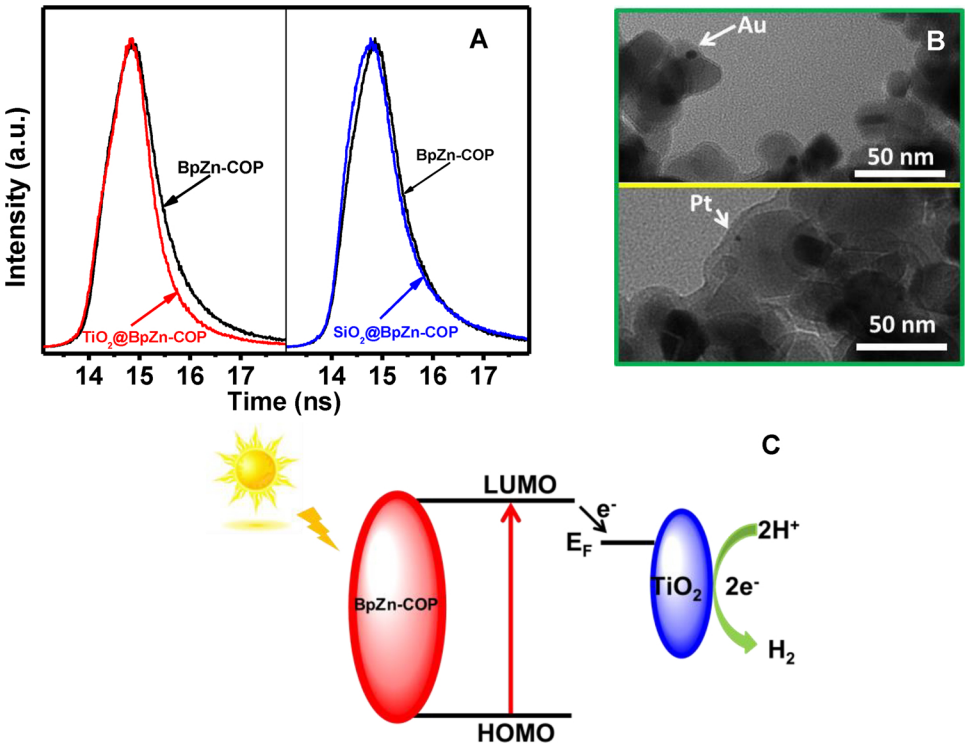

Fig. 7. (A) Time-resolved photoluminescence decay spectra at 600 nm obtained for the BpZn-COP, TiO_2@BpZn-COP-2.5% and SiO_2@BpZn-COP-2.5%, (B) TEM images of TiO_2@ BpZn-COP-2.5% after in-situ photodeposited with Au and Pt under visible light, (C) Schematic illustration of charge separation between polymer and TiO_2 in the composite TiO_2@ BpZn-COP.

the photocatalytic activity of the composite photocatalyst decreased slightly at second cycle, however, the photocatalytic activity can be then maintained after that. The possible reason for the decreased photocatalyic at the initial stage may be attributed to the exfoliation of a very small amount of pure polymer which were not intimately coated on the surface of TiO_2 surface although most of the polymers are well-coated. The TEM image of composite TiO_2@BpZn-COP-2.5% after long-time reaction shows that almost all the polymers still maintained and intimately coated on the surface of TiO_2, indicating the composite is very stable under the photocatalytic reaction condition.

4. Conclusion

In summary, the visible-light-driven H_2 production via water

splitting was successfully realized over novel bipyridine-based conjugated organic polymers, Bp-COP and BpZn-COP, which possess excellent light-harvesting properties with absorption edges expanding to more than 600 nm. Studies suggested that the presence of Zn(II) could efficiently promote the charge separation and transport, resulting in a higher photocatalytic activity. Further assembling TiO_2 with BpZn-COP could effectively migrate photoexcited electrons from polymer to TiO_2, as evidenced by TRPL and in-situ photodepositon probe reactions. Consequently, the photocatalytic activity of the composite was remarkably increased and an apparent quantum efficiency (AQE) could reach over 2.5% at the input wavelength of 420 nm. As far as we know, it is one of the efficient photocatalytic systems using porous organic polymers as candidates for photocatalytic water splitting. Our preliminary results indicate that photocatalytic activity of conjugated organic polymers could be efficiently modulated via optimizing not only their light absorption properties but also their charge separation and transport process. The work facilitates the designing of organic polymers with narrow band gaps for potential and promising applications in solar energy conversion and utilization.

Acknowledgements

We thank Ms Y. Xiao and Ms D. Tu for the discussion and help with CV test. This work was supported by the NSFC (21733009, 21232008, 21621063), Key Research Program of Frontier Sciences, CAS (QYZDY-SSW-JSC023) and the Strategic Priority Research Program of the Chinese Academy of Sciences (XDB17020200).

Appendix A. Supplementary data

Supplementary material related to this article can be found, in the online version, at doi:https://doi.org/10.1016/j.apcatb.2018.09.011.

References

[1] A. Fujishima, K. Honda, Eletrochemical photolysis of water at a semiconductor electrode, Nature 238 (1972) 37–38.
[2] J. Bard, M.A. Fox, Artificial photosynthesis: solar splitting of water to hydrogen and oxygen, Acc. Chem. Res. 28 (1995) 141–145.
[3] V.S. Vyas, V.W. Lau, B.V. Lotsch, Soft photocatalysis: organic polymers for solar fuel production, Chem. Mater. 28 (2016) 5191–5204.
[4] H. Liu, C. Xu, D. Li, H. Jiang, Photocatalytic hydrogen production coupled with selective benzylamine oxidation over MOF composites, Angew. Chem. Int. Ed. 57 (2018) 5379–5383.
[5] J. Xiao, H. Jiang, Thermally stable metal-organic framework-templated synthesis of hierarchically porous metal sulfdes: enhanced photocatalytic hydrogen production, Small 13 (2017) 1700632.
[6] Y. Zhu, Y. Wang, Q. Ling, Y. Zhu, Enhancement of full-spectrum photocatalytic activity over $BiPO_4/Bi_2WO_6$ composites, Appl. Catal. B-Environ. 200 (2017) 222–229.
[7] L. Zeng, X. Guo, C. He, C. Duan, Metal-organic frameworks: versatile materials for heterogeneous photocatalysis, ACS Catal. 6 (2016) 7935–7947.
[8] K. Maeda, K. Teramura, D. Lu, T. Takata, N. Saito, Y. Inoue, K. Domen, Photocatalyst releasing hydrogen from water, Nature 440 (2006) 295.
[9] J. Xie, S.A. Shevlin, Q. Ruan, S.J.A. Moniz, Y. Liu, X. Liu, Y. Li, C.C. Lau, Z.X. Guo, J. Tang, Efficient visible light-driven water oxidation and proton reduction by an ordered covalent triazine-based framework, Energy Environ. Sci. 11 (2018) 1617–1624.
[10] D.M. Schultz, T.P. Yoon, Solar synthesis: prospects in visible light photocatalysis, Science 343 (2014) 1239176.
[11] J. Xiao, L. Han, J. Lu, S. Yu, H. Jiang, Integration of plasmonic effects and schottky junctions into metal-organic framework composites: steering charge flow for enhanced visible-light photocatalysis, Angew. Chem. Int. Ed. 57 (2018) 1103–1107.
[12] X. Fang, Q. Shang, Y. Wang, L. Jiao, T. Yao, Y. Li, Q. Zhang, Y. Luo, H. Jiang, Single Pt atoms confned into a metal-organic framework for effcient photocatalysis, Adv. Mater. 30 (2018) 1705112.
[13] X. Tao, Y. Zhao, L. Mu, S. Wang, R. Li, C. Li, Bismuth tantalum oxyhalogen: a promising candidate photocatalyst for solar water splitting, Adv. Energy Mater. 8 (2018) 1701392.
[14] D.J. Woods, R.S. Sprick, C.L. Smith, A.J. Cowan, A.I. Cooper, A solution-processable polymer photocatalyst for hydrogen evolution from water, Adv. Energy Mater. 7 (2017) 1700479.
[15] S. Kuecken, A. Acharjya, L. Zhi, M. Schwarze, R. Schoma¨cker, A. Thomas, Fast tuning of covalent triazine frameworks for photocatalytic hydrogen evolution, Chem. Commun. 53 (2017) 5854–5857.
[16] Z. Li, J. Xiao, H. Jiang, Encapsulating a Co(II) molecular photocatalyst in Metal-OrganicFramework for visible-light-Driven H_2 production: boosting catalytic efficiency via spatial charge separation, ACS Catal. 6 (2016) 5359–5365.
[17] H. Li, Y. Zhou, W. Tu, J. Ye, Z. Zou, State-of-the-Art progress in diverse heterostructured photocatalysts toward promoting photocatalytic performance, Adv. Funct. Mater. 25 (2015) 998–1013.
[18] J. Zhou, Y. Lei, C. Ma, We. Lv, N. Li, Y. Wang, H. Xu, Z. Zou, A (001) dominated conjugated polymer with high-performance of hydrogen evolution under solar light irradiation, Chem. Commun. 53 (2017) 10536–10539.
[19] X. Wang, K. Meada, X. Chen, K. Takanabe, K. Domen, Y. Hou, X. Fu, M. Antonietti, Polymer semiconductors for artificial photosynthesis: hydrogen evolution by mesoporous graphitic carbon nitride with visible light, J. Am. Chem. Soc. 131 (2009) 1680–1681.
[20] X. Wang, K. Maeda, A. Thomas, K. Takanabe, G. Xin, J.M. Carlsson, K. Domen, M. Antonietti, A metal-free polymeric photocatalyst for hydrogen production from water under visible light, Nature Mater. 8 (2009) 76–80.
[21] S. Cao, J. Yu, G-C_3N_4-based photocatalysts for hydrogen generation, J. Phys. Chem. Lett. 5 (2014) 2101–2107.
[22] K. Schwinghammer, B. Tuffy, M.B. Mesch, E. Wirnhier, C. Martineau, F. Taulelle, W. Schnick, J. Senker, B.V. Lotsch, Triazine-based carbon nitrides for visible-light-driven hydrogen evolution, Angew. Chem. Int. Ed. 52 (2013) 2435–2439.
[23] D. Masih, Y. Ma, S. Rohani, Graphitic C_3N_4 based noble-metal-free photocatalyst systems: a review, Appl. Catal. B-Environ. 206 (2017) 556–588.
[24] M. Zhang, J. Xu, R. Zong, Y. Zhu, Enhancement of visible light photocatalytic activities via porous structure of g-C_3N_4, Appl. Catal. B-Environ. 147 (2014) 229–235.
[25] Y. Guo, S. Chu, S. Yan, Y. Wang, Z. Zou, Developing a polymeric semiconductor photocatalyst with visible light response, Chem. Commun. 46 (2010) 7325–7327.
[26] W. Xing, W. Tu, Z. Han, Y. Hu, Q. Meng, G. Chen, Template-induced high-crystalline g-C3N_4 nanosheets for enhanced photocatalytic H_2 evolution, ACS Energy Lett. 3 (2018) 514–519.
[27] Y. Liu, H. Zhang, J. Ke, J. Zhang, W. Tian, X. Xu, X. Duan, H. Sun, M.O. Tade, S. Wang, 0D (MoS_2)/2D (g-C_3N_4) heterojunctions in Z-scheme for enhanced photocatalytic and electrochemical hydrogen evolution, Appl. Catal. B-Environ. 228 (2018) 64–74.
[28] D. Chen, K. Wang, W. Hong, R. Zong, W. Yao, Y. Zhu, Visible light photoactivity enhancement via CuTCPP hybridized g-C_3N_4 nanocomposite, Appl. Catal. B-Environ. 166-167 (2015) 366–373.
[29] L. Stegbauer, K. Schwinghammer, B.V. Lotsch, A hydrazone-based covalent organic framework for photocatalytic hydrogen production, Chem. Sci. 5 (2014) 2789–2793.
[30] R.S. Sprick, J.X. Jiang, B. Bonillo, S. Ren, T. Ratvijitvech, P. Guiglion, M.A. Zwijnenburg, D.J. Adams, A.I. Cooper, Tunable organic photocatalysts for visible-light-driven hydrogen evolution, J. Am. Chem. Soc. 137 (2015) 3265–3270.
[31] G. Mukherjee, J. Thote, H.B. Aiyappa, S. Kandambeth, S. Banerjee, K. Vanka, R. Banerjee, A porous porphyrin organic polymer (PPOP) for visible light triggered hydrogen production, Chem. Commun. 53 (2017) 4461–4464.
[32] X. Huang, Z. Wu, H. Zheng, W. Dong, G. Wang, A sustainable method toward melamine-based conjugated polymer semiconductors for efficient photocatalytic hydrogen production under visible light, Green Chem. 20 (2018) 664–670.
[33] T. Banerjee, F. Haase, G. Savasci, K. Gottschling, C. Ochsenfeld, B.V. Lotsch, Single-site photocatalytic H_2 evolution from covalent organic frameworks with molecular cobaloxime Co-catalysts, J. Am. Chem. Soc. 139 (2017) 16228–16234.
[34] K. Wang, L. Yang, X. Wang, L. Guo, G. Cheng, C. Zhang, S. Jin, B. Tan, A. Cooper, Covalent triazine frameworks via a low-temperature polycondensation approach, Angew. Chem. Int. Ed. 56 (2017) 14149–14153.
[35] T. Banerjee, K. Gottschling, G. Savasci, C. Ochsenfeld, B.V. Lotsch, H_2 evolution with covalent organic framework photocatalysts, ACS Energy Lett. 3 (2018) 400–409.
[36] J. Park, Visible and near infrared light active photocatalysis based on conjugated polymers, J. Ind. Eng. Chem. 51 (2017) 27–43.
[37] L. Wang, Y. Wan, Y. Ding, S. Wu, Y. Zhang, X. Zhang, G. Zhang, Y. Xiong, X. Wu, J. Yang, H. Xu, Conjugated microporous polymer nanosheets for overall water splitting using visible light, Adv. Mater. 29 (2017) 1702428.
[38] G. Zhang, Z.A. Lan, X. Wang, Conjugated polymers: catalysts for photocatalytic hydrogen evolution, Angew. Chem. Int. Ed. 55 (2016) 15712–15727.
[39] R.S. Sprick, B. Bonillo, M. Sachs, R. Clowes, J.R. Durrant, Dave J. Adams, A.I. Cooper, Extended conjugated microporous polymers for photocatalytic hydrogen evolution from water, Chem. Commun. 52 (2016) 10008–10011.
[40] N. Chaoui, M. Trunk, R. Dawson, J. Schmidt, A. Thomas, Trends and challenges for microporous polymer, Chem. Soc. Rev. 46 (2017) 3302–3321.
[41] V.V.S. Vyas, F. Haase, L. Stegbauer, G. Savasci, F. Podjaski, C. Ochsenfeld, B.V. Lotsch, A tunable azine covalent organic framework platform for visible light-induced hydrogen generation, Nat. Commun. 6 (2015) 8508.
[42] P. Pachfule, A. Acharjya, J. Roeser, T. Langenhahn, M. Schwarze, R. Schomacker, A. Thomas, J. Schmidt, Diacetylene functionalized covalent organic framework (COF) for photocatalytic hydrogen generation, J. Am. Chem. Soc. 140 (2018) 1423–1427.
[43] R.S. Sprick, B. Bonillo, R. Clowes, P. Guiglion, N.J. Brownbill, B.J. Slater, F. Blanc, M.A. Zwijnenburg, D.J. Adams, A.I. Cooper, Visible-light-driven hydrogen evolution using planarized conjugated polymer photocatalysts, Angew. Chem. Int. Ed. 55 (2016) 1792–1796.
[44] L. Li, Z. Cai, Q. Wu, W.Y. Lo, N. Zhang, L.X. Chen, L. Yu, Rational design of porous conjugated polymers and roles of residual palladium for photocatalytic hydrogen production, J. Am. Chem. Soc. 138 (2016) 7681–7686.
[45] M. Zhong, H. Li, J. Chen, L. Tao, C. Li, Q. Yang, Cooperative activation of cobalt-salen complexes for epoxide hydration promoted on flexible porous organic

frameworks, Chem. Eur. J. 23 (2017) 11504–15508.
[46] M. Bhadra, H.S. Sasmal, A. Basu, S.P. Midya, S. Kandambeth, P. Pachfule, E. Balaraman, R. Banerjee, Predesigned metal-anchored building block for in situ generation of Pd nanoparticles in porous covalent organic framework: application in heterogeneous tandem catalysis, ACS Appl. Mater. Interfaces 9 (2017) 13785–13792.
[47] J. Chen, H. Li, M. Zhong, Q. Yang, Hierarchical mesoporous organic polymer with an intercalated metal complex for the efficient synthesis of cyclic carbonates from flue gas, Green Chem. 18 (2016) 6493–6500.
[48] C.H. Hendon, D. Tiana, M. Fontecave, C. Sanchez, L. D'Arras, C. Sassoye, L. Rozes, C. Mellot-Draznieks, A. Walsh, Engineering the optical response of the titanium-MIL-125 metal-organic framework through ligand functionalization, J. Am. Chem. Soc. 135 (2013) 10942–10945.
[49] K. Maeda, K. Ishimaki, Y. Tokunaga, D. Lu, M. Eguchi, Modification of wide-band-gap oxide semiconductors with cobalt hydroxide nanoclusters for visible-light water oxidation, Angew. Chem. Int. Ed. 55 (2016) 8309–8313.
[50] C. Huang, C. Chen, M. Zhang, L. Lin, X. Ye, S. Lin, M. Antonietti, X. Wang, Carbon-doped BN nanosheets for metal-free photoredox catalysis, Nat. Commun. 6 (2015) 7698.
[51] Z.A. Lan, Y. Fang, Y. Zhang, X. Wang, Photocatalytic oxygen evolution from functional triazine-based polymers with tunable band structures, Angew. Chem. Int. Ed. 57 (2018) 470–474.
[52] J. Zhang, Y. Chen, X. Wang, Two-dimensional covalent carbon nitride nanosheets: synthesis, functionalization, and applications, Energy Environ. Sci. 8 (2015) 3092–3108.
[53] Y. Wang, W. Yang, X. Chen, J. Wang, Y. Zhu, Photocatalytic activity enhancement of core-shell structure g-C_3N_4@TiO_2 via controlled ultrathin g-C_3N_4 layer, Appl. Catal. B-Environ. 220 (2018) 337–347.
[54] Y. Wang, W. Jiang, W. Luo, X. Chen, Y. Zhu, Ultrathin nanosheets g-C_3N_4@Bi_2WO_6 core-shell structure via low temperature reassembled strategy to promote photocatalytic activity, Appl. Catal. B-Environ. 237 (2018) 633–640.
[55] Y. Tan, Z. Shu, J. Zhou, T. Li, W. Wang, Z. Zhao, One-step synthesis of nanostructured g-C_3N_4/TiO_2 composite for highly enhanced visible-light photocatalytic H_2 evolution, Appl. Catal. B-Environ. 230 (2018) 260–268.
[56] Y.P. Xie, Z.B. Yu, G. Liu, X.L. Ma, H. Cheng, CdS-mesoporous ZnS core-shell particles for efficient and stable photocatalytic hydrogen evolution under visible light, Energy Environ. Sci. 7 (2014) 1895–1901.
[57] K. Zhang, J.K. Kim, M. Ma, S.Y. Yim, C. Lee, H. Shin, J.H. Park, Delocalized electron accumulation at nanorod tips: origin of effi cient H_2 generation, Adv. Funct. Mater. 26 (2016) 4527–4534.
[58] L. Huang, X. Wang, J. Yang, G. Liu, J. Han, C. Li, Dual cocatalysts loaded type I CdS/ZnS Core/Shell nanocrystals as effective and stable photocatalysts for H_2 evolution, J. Phys. Chem. C 117 (2013) 11584–11591.
[59] L. Huang, J. Yang, X. Wang, J. Han, H. Han, C. Li, Effects of surface modification on photocatalytic activity of CdS nanocrystals studied by photoluminescence spectroscopy, Phys. Chem. Chem. Phys. 15 (2013) 553–560.
[60] Q. Liu, Y. Guo, Z. Chen, Z. Zhang, X. Fang, Constructing a novel ternary Fe(III)/graphene/g-C_3N_4 composite photocatalyst with enhanced visible-light driven photocatalytic activity via interfacial charge transfer effect, Appl. Catal. B-Environ. 183 (2016) 231–241.